



Synthesis and characterization of hydrophobic glass-ceramic thin film derived from colloidal silica, zirconium(IV) propoxide and methyltrimethoxysilane via sol–gel method

Aykut Ak^{1,2} · Buğra Çiçek¹

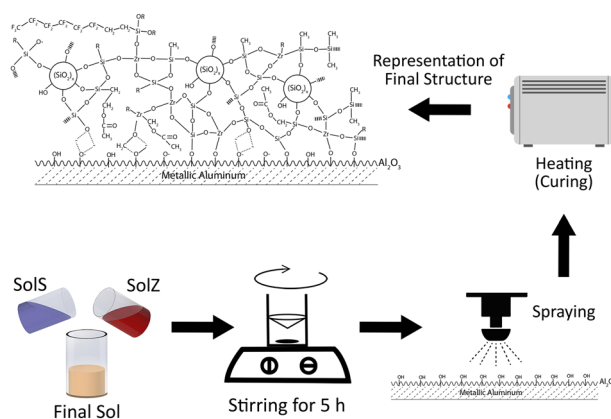
Received: 17 December 2020 / Accepted: 21 January 2021 / Published online: 19 February 2021

© The Author(s), under exclusive licence to Springer Science+Business Media, LLC part of Springer Nature 2021

Abstract

This study focuses on the synthesis and characterization of Zirconium(IV) Propoxide (ZTP), Colloidal Silica (CS), and Methyltrimethoxysilane (MTMS)-derived non-stick hard coatings prepared via the sol–gel method. In the synthetic procedure, two different solutions were prepared separately based on the different hydrolysis rates of the silicon (SolS) and zirconium (SolZ) components. Polydimethoxysilane (PDMS) and Fluoralkylsilane (FAS) were used as hydrophobicity-promoting agents. The solution was applied onto aluminum surface, which was afterward dried and densified at 250 °C. The final solution was characterized by FTIR spectroscopy to determine the Zr–O–Si hetero-bonding and Si–O–Si and Zr–O–Zr homo-bonding. Coatings were analyzed by their hardness, hydrophobicity, and gloss. A homogeneous solution and crack-free hybrid coating was obtained. FTIR results showed that homo- and hetero-bonding between Zr and Si elements were obtained from a precipitation-free solution. Measured contact angles varied between 100° and 112°, and these results were evaluated according to the surface and gel structure.

Graphical Abstract



Keywords Colloidal silica · Zirconium tetrapropoxide · Hydrophobicity · Aluminum Corrosion · Hybrid sol–gel

✉ Buğra Çiçek
bcicek@yildiz.edu.tr

¹ Department of Metallurgical and Materials Engineering, Yıldız Technical University, 34210, Esenler, Istanbul, Turkey

² Akcoat R&D Center, Enamel Coatings Division, 2nd IZ, 54300, Hendek, Sakarya, Turkey

Highlights

- A crack-free, hydrophobic, hard hybrid thin films were synthesized using ZTP, MTMS and CS via sol–gel method.
- ZTP increased the contact angle of the film surface.
- Precipitation-free SolS solution was obtained due to the reactions between methyl groups in MTMS and the colloidal silica particles.
- PDMS and FAS components further increased the wetting angle of the hybrid film up to a specific ratio.
- FTIR results showed that Zr–O–Si hetero-bonding and Si–O–Si, Zr–O–Zr homo-bonding were obtained as result of the precipitation-free solution.

1 Introduction

Hybrid coatings are nano-composite materials consisting of both inorganic and organic components together. They are often used to decrease or prevent chemical and physical corrosion of metallic surfaces [1, 2]. Some metallic materials such as aluminum have a thin protective oxide film (Al_2O_3) on the surface that protects against corrosion deriving from its natural oxidation, but even this can be corroded under harsh conditions, and this corrosion can give rise to health problems or economic damages [3, 4]. In one of the most common examples of this process, aluminum contamination can take place from cookware to food via chemical and/or mechanical means. This contamination might accumulate in the human body and cause various health problems [3, 5–7], of which Alzheimer's disease is the most commonly known [8, 9]. Hybrid coatings can both prevent contamination by creating a barrier and provide a non-stick surface that improves the cooking and cleaning properties of cookware. This work is based on the synthesis of hydrophobic cookware coatings.

The sol–gel method is a well-known technique for producing bulk glasses, ceramics, aerogels, fibers, nanopowders and hybrid coatings [10–13]. In particular, hybrid coatings prepared by this method have many advantages arising from the combined inorganic and organic structure [12]. Also, sol–gel coatings adhere well to various material surfaces such as wood, most metals, glass and polymers [14–16].

The fundamental process of preparing sol–gel coatings consists of two basic steps: colloidal solution preparation and gelation of this solution [17]. The solution is obtained by mixing metal alkoxide, solvent, catalyst, and water in a specific order, as detailed in the experimental section. During mixing, hydrolysis and condensation reactions take place simultaneously and –Me–O–Me– bonds occur, accompanied by a catalyst to provide control. This bonding process is called Gelation [18]. The sol–gel process is very sensitive to environmental conditions such as the type of catalyst, pH, temperature, viscosity, and gelation time [17, 18].

Large number of studies were carried out to investigate the prevention of aluminum corrosion. Milosev et al. and

Rodič et al. worked on preparing hybrid coatings to serve as a barrier for corrosion protection of aluminum using zirconium(IV) propoxide (ZTP) as a zirconium (Zr) source and various silicon (Si) sources [19–22].

There are comprehensive descriptions about stabilization and hybridization of Zr and Si metal alkoxides made by Schubert [23, 24]. Also, he studied with carboxylic acids ($\text{R}'\text{COOH}$) such as acetic acid to tune the reactivity of transition metal alkoxides such as $\text{Zr}(\text{OR})_4$ compounds [24].

Villegas *c* evaluated the influence of the thermal densification degree of Zr–Si coatings and determined the main factors affecting the hydrolytic resistance of the coatings.

Del Monte et al. [25] prepared crack-free films using TEOS, ZTP, and Titanium(IV). Isopropoxide, and confirmed that both Titanium- (Ti) and Zr-based ormosils can be fabricated with high optical quality.

Regarding the cookware, Jeon and Kim [26] defined a non-stick ceramic coating composition and process for cookware using colloidal silica (CS), MTMS, and FAS.

Ugur et al. [27] described a preparation similar to that of Jeon and Kim, with additional dopants.

Baney et al. [28] prepared an abrasion-resistant hard coating composition comprising an acidic dispersion of colloidal titania.

Works on decreasing or blocking corrosion with zirconium-toughened silicon coatings have been carried out for other sectors besides cookware. However, there are no publications regarding CS–metal alkoxide interactions. Besides, most of these works ignore the hydrophobicity of the surface, which is very important for the corrosion protection, because interactions between the surface and wet environments are affected by surface tension [29]. Carre et al. [30] describe a process for preparing a non-stick, abrasion-resistant cookware surface containing zirconium alkoxide and diethoxydimethylsilane as the silicon source. Yet, their silane sources are different from those of this work. In the present paper, the effect of ZTP on hydrophobic CS–Methyltrimethoxysilane (MTMS) thin films is elucidated. Metal alkoxides were used as the sources of Zr and Si. The effect of Zr on the film body was analyzed via changing the Zr/Si ratio.

2 Experimental

2.1 Materials

A 3003 series aluminum alloy was used as a substrate. Before the coating, the surface of the substrate was pre-treated as described in the following sections.

The following precursors were used as sol–gel starting materials: MTMS ($\text{CH}_3\text{Si}(\text{OCH}_3)_3$, 98%, Sigma); CS (30%, Ludox HS–30, Sigma-Aldrich); Glacial Acetic Acid (Hac: CH_3COOH , 100% anhydrous, Isolab); Zirconium(IV) propoxide (ZTP: $\text{Zr}(\text{OCH}_2\text{CH}_2\text{CH}_3)_4$, 70 wt.% in 1-propanol, Sigma); polydimethylsiloxane (PDMS: average mw ~ 550 , viscosity ~ 25 cSt, Sigma-Aldrich); 1H,1H,2H,2H-perfluorooctyltrimethoxysilane (FAS: $\text{C}_{11}\text{H}_{13}\text{F}_{13}\text{O}_3\text{Si}$, 97 wt.%, ABCR); distilled water (H_2O).

2.2 Preparation of the hybrid coating

Silicon- and zirconium-based solutions were synthesized separately as SolS and SolZ. SolS was prepared by mixing MTMS and Hac with a mole ratio of 1:1.064 and stirring at 150 rpm for 15 min, as shown in Fig. 1. Subsequently, CS was added to the solution by dropwise under stirring. With the addition of CS, the white milky suspension turned into a transparent solution and the beaker slightly warmed. The MTMS/CS ratio was calculated as the dry weight ratios of MTMS and CS from the $\text{CH}_3\text{SiO}_3/2$ and SiO_2 formulations. This ratio is generally chosen between 40:60 and 60:40 to obtain a transparent glass body [31–33]. The dry weight ratios of MTMS and CS investigated were as follows: $\text{CH}_3\text{SiO}_3/2:\text{SiO}_2 = 60:40, 50:50, 40:60$. In the present work,

the 50:50 composition was chosen after preliminary results with respect to surface morphology. This solution was named SolS and left for 45 min under stirring. Meanwhile, SolZ was prepared by mixing different amounts of ZTP with Hac, PDMS, and FAS. ZTP and Hac were set with constant molar ratio: 1:5.7. PDMS was added to the SolZ at different weight % according to the total weight of the final sol. The whole recipe is presented in Table 1. ZTP, Hac, PDMS, and FAS were mixed at 120 rpm for 30 min and then distilled water added to SolZ by dropwise addition with the mole ratio of $\text{ZTP}:\text{H}_2\text{O} = 1:5$, followed by stirring for 10 more minutes. After partial hydrolysis with water, the cloudy solution turned clear. Subsequently, The SolZ was added to the SolS by dropwise under stirring. This final solution was stirred at 300 rpm for 5 h to allow gelation to occur. All these reactions were performed under acidic conditions, with pH generally kept under 4.5. The pH of the blend (Final Sol) was between 3.4 and 3.8. After adding the chemicals into a 100 ml beaker, the top of the beaker was

Table 1 Theoretical molar ratios of the different components in the sol–gel hybrid coating, assuming a 100% cross-linking degree

Experiment	Zr/Si (mole rate)	PDMS (% mass)	FAS/Zr (mole rate)
B06	0.06	1.5	–
B12	0.12	1.5	–
B24	0.24	1.5	–
B48	0.48	1.5	–
BP12.3	0.12	3.5	–
BP12.5	0.12	5.5	–

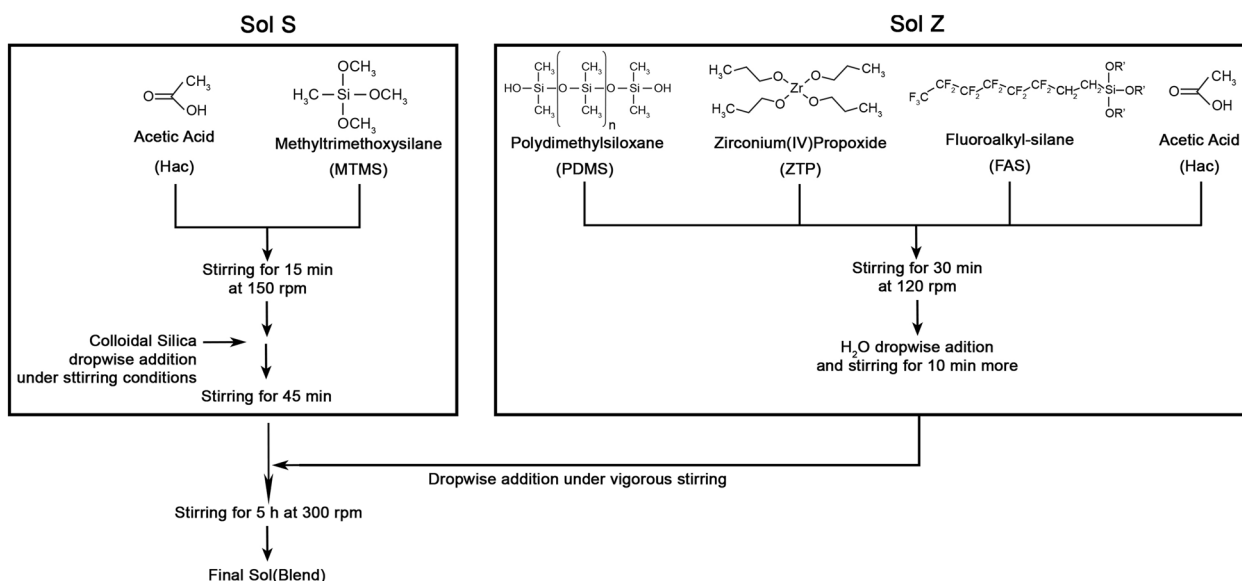


Fig. 1 Preparation flowchart of the final solution

covered with a paraffin sheet to exclude air during the reaction.

Three types of experiments were performed: varying the Zr/Si ratio, varying the PDMS amount, and the effect of FAS addition. The Zr/Si ratios were chosen as 0.06, 0.12, 0.24, and 0.48. These solutions were named as B06, B12, B24, and B48, respectively. The amounts of PDMS used in the experiments were 1.5, 3.5, and 5.5 wt.%. The solutions with extra PDMS were named as BP12.3 and BP12.5. The sample with FAS/Zr:0044 mole rate was named as BF12.1. Before applying the coating, dust, and oil were removed from the substrate using trichloroethylene or acetylacetone. Then a sandblasting procedure was applied as described in detail by Jeon and Kim [26]. The pre-treated substrate was heated between 45 and 65 °C [26, 27]. The gelled blends were applied onto the pre-treated aluminum surface by the spraying method. Spraying parameters described by Ugur et al. were used to obtain homogenous and reproducible surfaces [27]. Coated samples were dried at 130° for 7 min, and densified at 250 °C for 15 min. Film thicknesses were kept between 30 and 35 μm. Each solution was applied onto three substrates to obtain the standard thickness and confirm the other surface properties.

2.3 Characterization

The bonding types in the chosen solutions was identified using a Perkin Elmer Fourier-transform infrared (FTIR) spectrometer in the wavelength range between 400 and 4000 cm^{-1} . The fundamental process that occurs in making the gel is attributed to the bonding between Si–O–Si, Zr–O–Si, and Zr–O–Zr. Hardness was measured using a Pencil Hardness apparatus according to the ISO 15184:2020 Standard. Koh-i-Noor Hardtmuth brand pencils are used with hardness from 8B to 10H. Hardness evaluation is one of the most important aims of this work, since the hardness reflects the efficiency and the strength of the bonding and the curing. Also, it is related to the lifespan and durability of the surface. Another important parameter in this work is the contact angle. Measuring the contact angle of a drop on the sample surface is the most practical way to characterize the surface tension between solid–vapor and solid–liquid phases [34]. The contact angle meter measures the surface tension against liquid according to the static method of the ISO 19403-2:2020 standard. Contact angle of an uncoated aluminum substrate was also measured to evaluate the effect of the coating. The OneAttension program was used for the measurement. Contact angles were determined by taking the average of the contact angles measured from five different positions of each sample.

Surface refractivity was probed by a TQC Sheen Polygloss glossmeter. Finally, the cross-cut test was

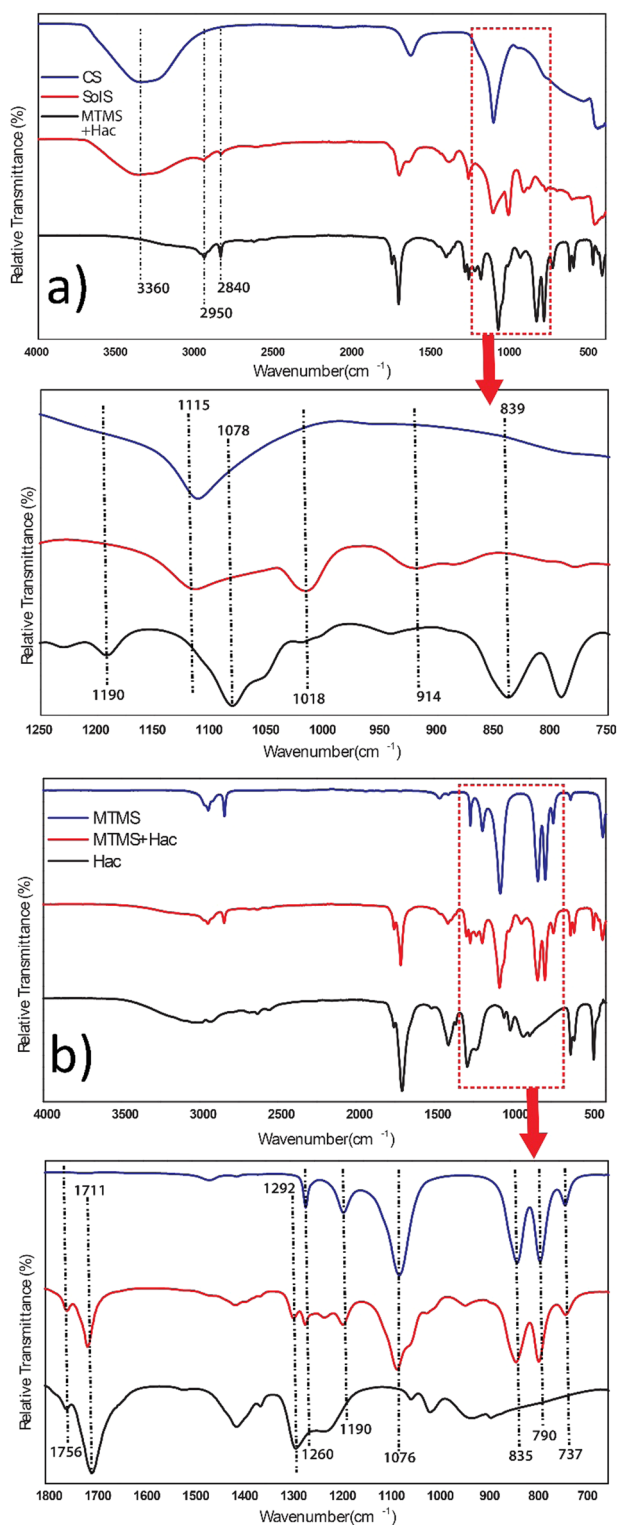


Fig. 2 **a** FTIR spectra of SolS solution with its components. **b** FTIR spectra of hydrolyzed MTMS + Hac solution with CS to determine whether new bonds are formed

applied for each sample to inspect the adherence level of films, with values ranging from 0 to 5 according to ISO 2409:2013 standard.

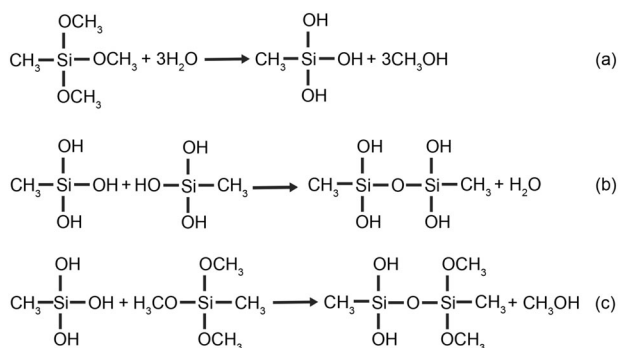


Fig. 3 Hydrolysis and condensation reactions of MTMS. Hydrolysis (a), water condensation (b), alcohol condensation (c)

3 Results and discussion

3.1 FTIR analysis

The nature of the bonding in SolS, SolZ, and the Final Sols was characterized by FTIR analysis. The partial gelation in both solutions can be observed in the spectra. Gelation in this work is defined as the formation of a continuous network made of Si–O–Si, Zr–O–Zr homo-condensation and Si–O–Zr hetero-condensation. Efficient gelation can be tracked by the presence and intensity of the corresponding bands. For all scans performed in this work, there were two kinds of spectra investigated in the region over 1755 cm^{-1} . Figure 2a depicts the synthesis of SolS by hydrolysis and condensation under acidic conditions. The broad band around 3360 cm^{-1} corresponds to stretching of various –OH groups in Fig. 2a [35]. Sharp bands at 2950 and 2840 cm^{-1} correspond to C–H stretches [36].

SolS has three components: MTMS, Hac, and CS. The most intense IR bands in MTMS are those at 1260 , 1190 , 1076 , 835 , 790 , and 737 cm^{-1} as seen in Fig. 2b.

Another component, Hac, has characteristic absorbance bands at 1756 , 1711 , 1292 cm^{-1} . After stabilization of MTMS with Hac, CS was added dropwise to the solution. The solution was turned milky white for 5 s, and then became transparent again. The heat generated in this part of the reaction is a sign of the presence of an exothermic reaction. As a result, new bands appeared at 1115 , 1018 , and 914 cm^{-1} which corresponded to the Si–O–Si and Si–OH bonds [37]. In addition, important reductions were observed at 1190 , 1078 and 839 cm^{-1} corresponding to Si–C, Si–O and Si–O–C bonds as demonstrate at Fig. 2a [33].

The hydrolysis of MTMS must have triggered condensation reactions. These two reactions generally occur simultaneously [18]. This means that if there is hydrolysis in some area, condensation will occur under acidic conditions.

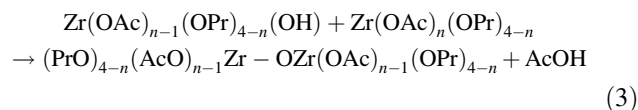
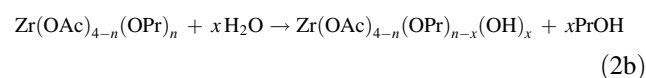
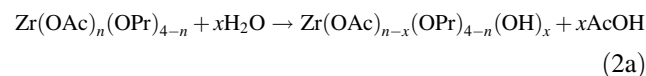
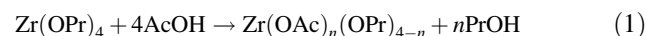
The hydrolysis reaction mechanism can be seen in Fig. 3a, and then alcoxolation (c) and oxalation (b) condensation

reactions take place. Most of the hydrolysis and condensation reactions occurred after the addition of CS because of the 70 wt.% water in the CS. Thus, MTMS became attached to the SiO_2 particles and condensed to form a siloxane network, and the SiO_2 ceramic particles entered the amorphous organic matrix as represented in Fig. 4. Also, hydrolyzed metal alkoxides provide a means for chemical bonding to the aluminum surface [38, 39].

The protective alumina film on aluminum is a semiconductor and the wet acidic solution causes activation and hydrolysis of the Al_2O_3 surface [40, 41]. Hence, chemical bonding occurs between the alumina surface and thin film, as shown in Fig. 4. Figure 4 represents the film, the substrate and the interface bonding structure according to various references [12, 26, 33, 41–44].

In addition, the sandblasting process carried out before applying the solution to the surface increases the surface area of the aluminum and provides extra mechanical holding force. As a result of both types of bonding, a strong adhesion mechanism takes place between the thin film and the alumina surface.

Figure 5 shows the IR spectrum of SolZ. Because of the reactivity of ZTP, SolZ tends to undergo rapid condensation. For this reason, the metallic center of ZTP was chelated with Hac. The characteristic IR bands of ZTP are at 1071 , 1128 , and 1155 cm^{-1} . Three new bands at 1451 , 1554 , and 1236 cm^{-1} appeared in the ZTP + Hac mixture that were not observed in the ZTP and Hac raw materials, as seen at Fig. 5a. Therefore, these bonds are attributable to a new compound formed during the reaction between ZTP and Hac [21].



It has been reported that the bands at 1236 and 1554 cm^{-1} correspond to the asymmetric stretch of the carbonyl group attached to the Zr ions, which can be represented as ZTP–AcOH (Eq. 1) [21, 25]. The band at 1236 cm^{-1} in the ZTP–Hac mixture shifted to 1266 cm^{-1} after hydrolysis (Eqs. 2a, 2b). Also, the 1451 cm^{-1} band is attributable to the compound $\text{Zr}(\text{OAc})_4$ [21]. While these bands increase, 1138 and 1451 cm^{-1} bands decrease and/or disappear. Evidence

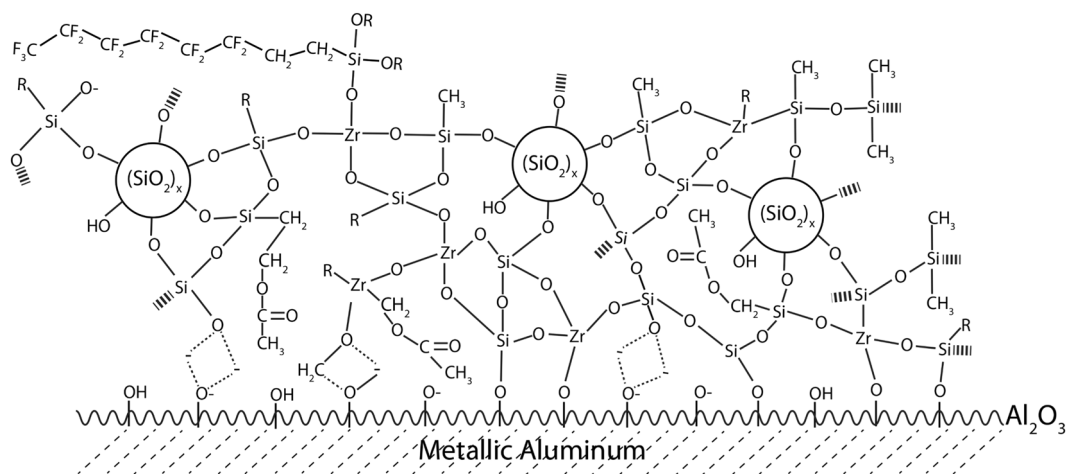


Fig. 4 Schematic representation of film structure and interface between substrate and film

of the hydrolysis of ZTP can be seen from changes in the ZTP bands at Fig. 5b.

The band at 1128 cm^{-1} can be assigned to Zr-O-C [21]. This band shifted to 1138 cm^{-1} and decreased after mixing with Hac. After the hydrolysis with H_2O , this band almost disappeared, as seen in Fig. 5b. This hydrolysis could cause condensation reactions in the presence of acetic acid (Eq. 3) [24]. The band at 1155 cm^{-1} also disappeared or became overlapped by the 1138 cm^{-1} band in the MTMS-Hac solution. In SolZ, experiments with and without PDMS did not show new bands as presented in Fig. 6a.

On the other hand, in the SolZ spectrum of BF12.1 in Fig. 6b, there was a new band that was not due to FAS. A small band at 1160 cm^{-1} is attributable to Si-O-Si and/or Si-O-Zr bonds [22].

Figure 7(a) displays the FTIR spectra of samples B06, B12, B24, and B48 that consist different Zr/Si ratios. Minor changes are detected in the region of $1600\text{--}900\text{ cm}^{-1}$. An increase in intensity at 1554 cm^{-1} band is observed by increasing the Zr/Si ratio related to ZTP-Hac complex as pointed out before. Bands at 1070 and 1050 cm^{-1} are assigned to ZTP. Also the bands at 960 cm^{-1} corresponds to Si-OH/ and/or Si-O-Zr bonds [19, 37]. Figure 7b shows the FTIR comparison of the B12 composition and its components, SolS and SolZ. As a result of detailed investigations, it was observed that the B12 mixture did not create a new band different from the components of the FTIR bands, overlapped with another large band, if any, or could not be detected by the device.

ZTP chelated with Hac, so that the metallic centers of ZTP remained stable. This means that uncontrollable rapid condensation was blocked. The absence of bands related to ZrO_2 precipitation in the FTIR results in the region around 500 cm^{-1} can be considered as a proof of the efficiency of metallic center stabilization and control of condensation

[45, 46]. Also, there are no new bands in that area different from ZTP bands after the chelating and hydrolysis processes. The high rate of hydrolysis was proved by the IR analysis. In addition to these results, an exothermic reaction occurred after mixing the ZTP, PDMS, and Hac. From these findings, the presence of homo-condensation (Zr-O-Zr) and hetero-condensation (Zr-O-Si) products of ZTP can be deduced [18, 23, 25, 37] (see discussions).

3.2 Water contact angle analysis

The optical images of water drop on coated and uncoated aluminum were exhibited in Fig. 8. Also, for clear comparison, a graph of the results is shown in Fig. 9. Three types of comparison are made in the same graph. The first solid line shows the results of tests with varying Zr/Si. It is clear that surface tension increases with the increase in the amount of zirconium. For a 100% increase in the Zr/Si ratio from 0.12 to 0.24, hydrophobicity degree rises about 2%. When the Zr/Si ratio was chosen as 0.48, the contact angle measured as 112° , with a 12% rise. Contact angle increase can be attributed to the changes in surface chemistry and/or changes in surface roughness.

As the Zr/Si ratio increases, the number of $-\text{CH}$ methyl groups also increase due to the amount of organic matter in the structure. The increase of surface tension can be attributable to the increase in the number of these $-\text{CH}$ groups. Next, BP12.3 and BP12.5 experiments were conducted by adding extra PDMS to the B12 formula. Thus, the three samples contain 1.5, 3.5, and 5.5 wt.% PDMS. The rest of the sample formulation was kept same. Considering the contact angle results, BP12.3 was determined to be more hydrophobic than B12. PDMS, which enters the film body structure increases the hydrophobicity due to the high amount of methyl groups it contains [47, 48]. PDMS

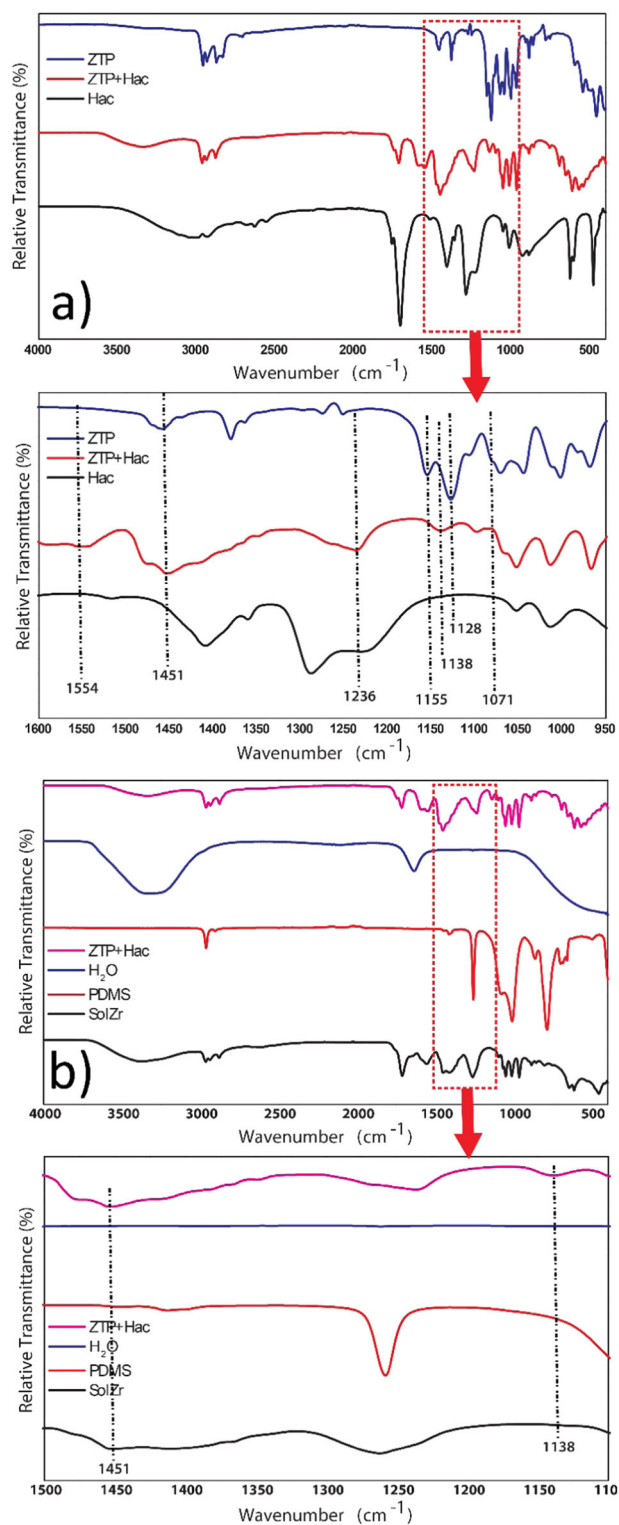


Fig. 5 **a** FTIR spectra of ZTP + Hac solution with its components, to observe bonds between ZTP and Hac. **b** FTIR spectra of SolZ, PDMS, H₂O, and ZTP + Hac sol to determine if new bonds are formed

addition of 2% with respect to the total mass resulted a hydrophobicity increase of 7.8%. However, in BP12.5, which has the highest PDMS ratio, the contact angle

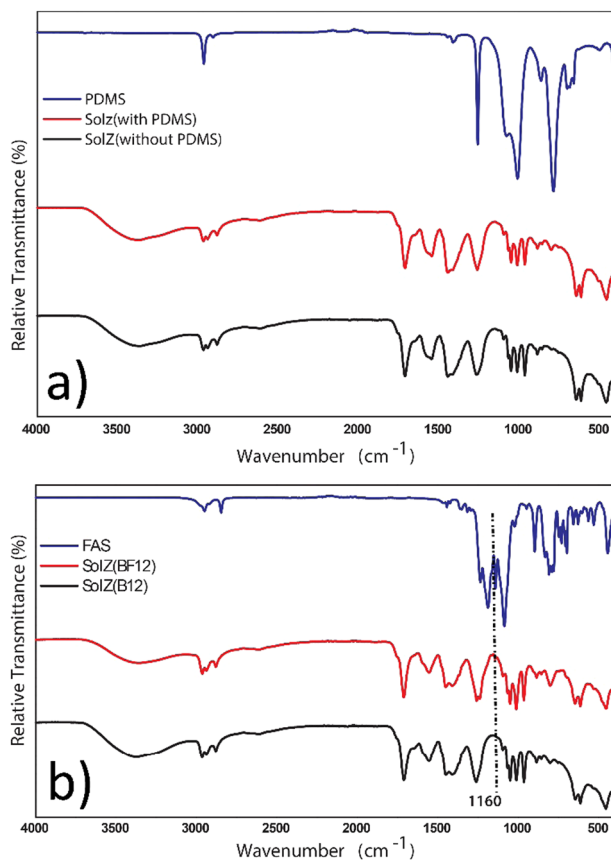


Fig. 6 **a** FTIR spectra of SolZ with and without PDMS to see if PDMS forms bonds with ZTP. **b** FTIR spectra of SolZ with and without FAS to determine if new bonds are formed

decreased by 5% compared to BP12.3. Examining the behavior of the solution during the experiment contributed greatly to our understanding of the reason for this decrease. While SolZ solutions of B12 and BP12.3 were homogeneous, BP12.5 became a heterogeneous emulsion and undissolved oil (PDMS) particles were observed on the surface of the solution. This suggests that there is a critical saturation rate for SolZ solution with respect to PDMS, and this rate is between 3.5 and 5.5 wt.%. For higher concentrations, PDMS passes the saturation point and separates from the SolZ by coalescing with other unreacted PDMS molecules.

Last, the FAS compound was added to the BF12 experiment such that $FAS / Zr = 0.044$. FAS supposed to reduce surface tension due to the fluorinated groups it contains [49]. As can be seen in Figs. 8 and 9, the hydrophobicity of the FAS-containing structure increased by about 5%. It was proved in a previous study that the fluorine/silicon (F/Si) ratio has an effect on hydrophobicity [50]. According to Izumi et al., as the F/Si ratio increases, the water repellency increases. It is notable that, in this work, the FAS composition was chosen as $F/Si = 13$.

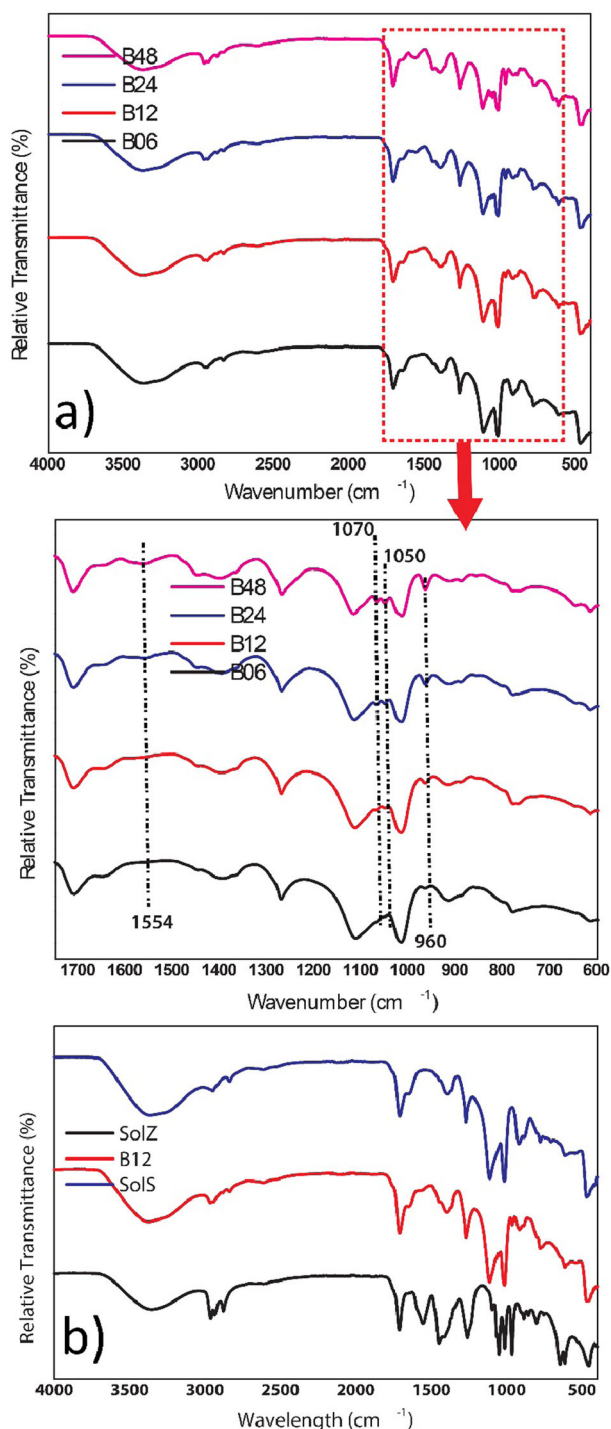


Fig. 7 **a** FTIR spectra of B06, B12, B24, and B48 to demonstrate effect of increase in Zr/Si ratio on bond intensities. **b** FTIR spectra of SolZ, SolS, and B12

3.3 Physical and mechanical properties

The hardness and the adherence of hydrophobic glass-ceramic thin films were represented in Table 2. The reflectivity (gloss) measurement results of coatings was

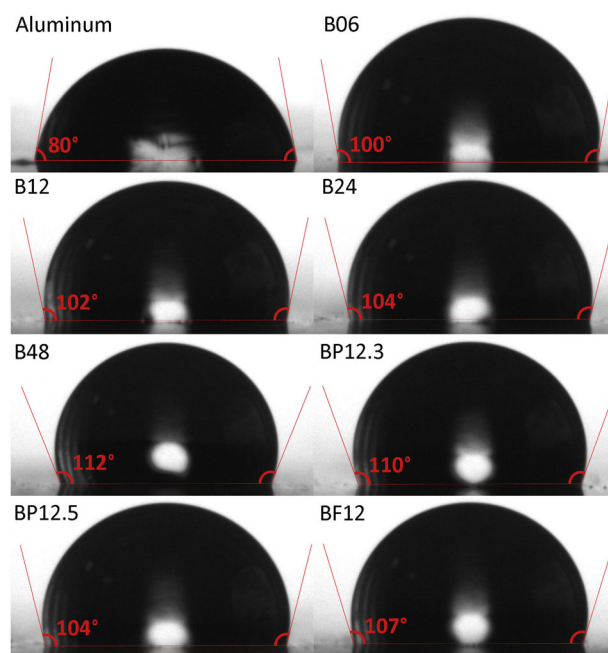


Fig. 8 Optical images of water drops of uncoated (aluminum) substrate and coated specimens (B06, B12, B24, B48, BP12.3, BP12.5, BF12)

demonstrated in Fig. 10. According to the test results, the sample with the lowest Zr/Si ratio (B06) provided the highest reflectivity as 30°. When the Zr/Si ratio was escalated to 0.12, the gloss decreased by 53% (to the 14°) as seen in Fig. 10. Also, even a 100% increase in the Zr/Si ratio from 0.12 to 0.24, the gloss decreased only 14%. When 3.5 wt.% PDMS is added to the base solution (BP12.3), the gloss increased from 14° to 24°. Further increasing the PDMS ratio to 5.5 wt.%, increased the reflectivity from 14° to 17° only. We assume that exceeding the threshold value PDMS coalesces to form a separate phase. Gloss meter measures the reflected light from the surface. The most important parameter that prevents reflection is the surface roughness [51]. Based on this, the surface roughness increases with an increase in the Zr/Si ratio, and an anti-reflective surface is formed. The roughness decreases up to a certain wt.% in PDMS, and then increases. Since the gloss value of the BF12 trial is the same as B12, it can be concluded that the presence of the FAS compound has no effect on surface gloss in this experiment.

Hardness is one of the most important parameters for the durability of protective coatings. B12 and BF12 specimens exhibited the highest hardness (9H) compared to other samples. As stated in the standard, the 9H pencil did not leave any permanent marks on these coatings but 10H pencil creates a plastic deformation on the film. After the B12 specimen, as Zr/Si increases, the hardness decreases rapidly to F. In the B06 coating, the hardness was obtained as H. The B06 specimen was the coating containing the highest inorganic/organic fraction, having the most solid

Fig. 9 Water contact angle results vs. Zr/Si ratio (solid line), PDMS amount (dashed line) and FAS effect (dotted line)

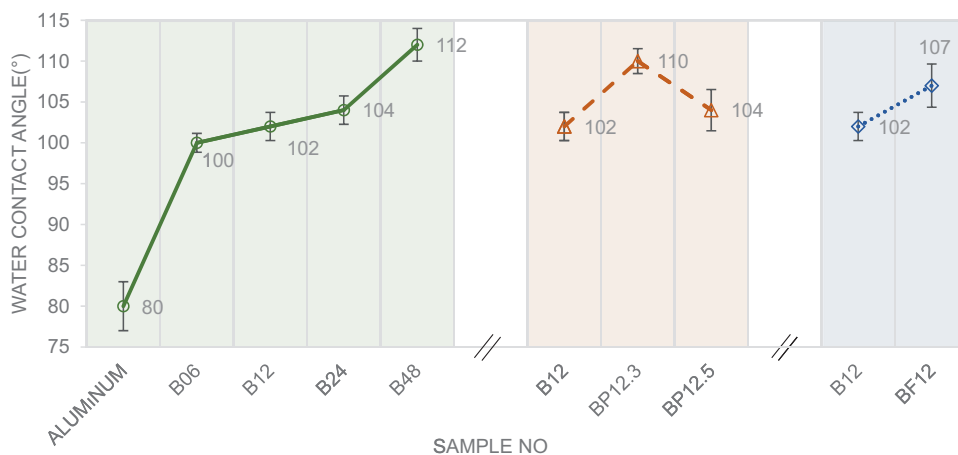


Table 2 Physical and mechanical properties of coatings

Sample	Pencil hardness	Cross cut
B06	H	0
B12	9H	0
B24	2H	0
B48	F	0
BP12.3	4H	0
BP12.5	H	0
BF12	9H	0

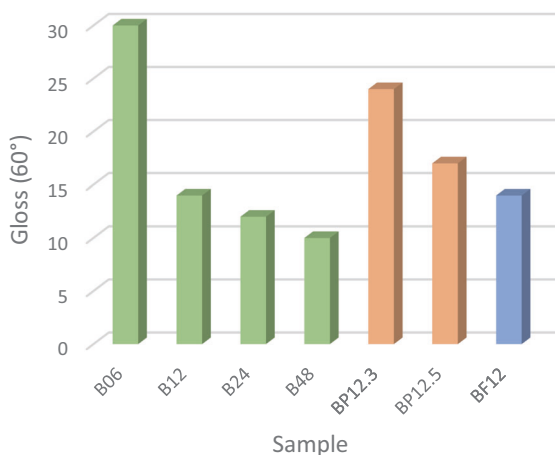


Fig. 10 Reflectivity (gloss) measurement results of samples

SiO₂ crystals. The cross-linking degree in B06 may not be as high as in B12 and B24, because the structural strength of the coating increases due to the efficiency of hydrolysis and condensation reactions in sol–gel films [52]. In other words, SiO₂ solid particles in the B06 structure may have prevented the conversion of Si–O–Si, Si–O–Zr, and Zr–O–Zr bonds.

Actually, CS nanoparticles have highly reactive silanol groups that may promote highly branched covalently

bonded siloxane networks [33]. Therefore, as the fraction of inorganic (SiO₂)/organic (MTMS + ZTP) in a sol–gel hybrid coating decreases, the structural durability decreases. Zr/Si = 0.12 ratio provides the best inorganic/organic ratio for the structural durability. In the PDMS tests, the BP12.3 experiment with 3.5 wt.% PDMS reached 4H and BP12.5 reached H hardness with 5.5 wt.% PDMS. When we compare these results with the result of B12, it can be clearly seen that the hardness decreases with increasing PDMS amount. This result is not surprising, because the PDMS is known as a soft hydrophobic additive [53]. This softening reduces stress in the thin film structure, preventing cracks [54]. Thus, the optimum PDMS ratio for synthesizing both a crack-free and hard coating was determined as the B12 sample with 1.5 wt.% PDMS.

According to the results of the adhesion test, all sol–gel hybrid coatings showed very good adhesion performance with the aluminum substrate. All coatings were in class 0 according to the ISO 2409:2013 standard, owing to efficient hydrolyzation of the metal alkoxides. Metal alkoxides are generally very reactive materials, especially against moisture. Even the moisture in the air can interact with metal alkoxides and cause precipitation. Zirconium alkoxides and silicon alkoxides have different reactivities; hence, their condensation and hydrolysis rates are different [55, 56].

ZTP generally reacts faster than MTMS. When both of these materials are mixed, heterogeneous clusters will be observed in the body [19, 43, 55]. Thus, two different solutions were prepared based on Si and Zr and these solutions were partly gelled for different lengths of time to overcome the activation difference problem. For the silicon-based solution, MTMS organoalkoxysilane was chosen as the silicon alkoxide because its water repellent nature derives from its methyl groups [57]. On the other hand, the OH groups on the surface of CS particles react with those methyl groups in MTMS. So, CS particles enter the structure due to this surface reaction [26]. Also, MTMS can undergo a condensation reaction with itself [58].

On the other hand, these hydrolysis and polymerization reactions generate alcohol as a by-product. Therefore, adding an extra solvent is unnecessary if the viscosity of the gel is low enough for efficient mixing. In the zirconium-based solution, a chelating agent must be used to prevent rapid condensation and stabilize the metallic center [55]. Acetic acid (Hac) is a good controllable acid for both solutions [26]. At the same time, acids can be used as a catalyst. The hydrophobic properties of OH-terminated PDMS are very high. Also it provides flexibility to the coating and reduces the cracking, which is critical for obtaining good mechanical properties [26, 27]. Cracks in the film body could be a result of the hard inorganic network causing stress accumulation, which could cause cracks in the film body [20, 21]. At this point, the organic matrix in the hybrid coating gives flexibility to the film body so the stress will not accumulate, and the cracking will be reduced [22–24].

4 Conclusion

A crack-free, hydrophobic, hard thin films were synthesized using ZTP, MTMS, and CS via the sol–gel method. Approximately 30- μm -thick films were applied onto a 3003 series aluminum substrate. FTIR results showed that Zr–O–Si hetero bonding and Si–O–Si, Zr–O–Zr homo bonding were obtained as result of the precipitation-free solution. Addition of the FAS agent only increased the wetting angle by about 5%. The purpose of use will determine whether the benefit of this improvement is worth the cost. On the other hand, the low-temperature curable structure makes current procedure an eco-friendly method. Despite densification temperatures as low as 250 °C, the inorganic network in the film body provides a relatively hard structure. This adhesive and hard surface resists scratches and keeps the film body stable. Also, the ratio between the MTMS and the SiO₂ nanoparticles is another critical parameter in producing transparent, crack-free and hard films.

Based on this study, it was shown that an increase in the non-stick and surface hardness properties can be transferred to strengthen the cookware coating and other anti-corrosive coating formulations. Achieving a desirable gloss change can also be applicable for the field of anti-reflective films.

Compliance with ethical standards

Conflict of interest The authors declare no competing interests.

Publisher's note Springer Nature remains neutral with regard to jurisdictional claims in published maps and institutional affiliations.

References

- Perrin FX, Ziarelli F, Dupuis A (2020) Relation between the corrosion resistance and the chemical structure of hybrid sol-gel coatings with interlinked inorganic-organic network. *Prog Org Coat* 141:105532. <https://doi.org/10.1016/j.porgcoat.2019.105532>
- Figueira RB, Sousa R, Silva CJR (2020), Multifunctional and smart organic–inorganic hybrid sol–gel coatings for corrosion protection applications, In: Makhoulf ASH, Abu-Thabit NY (eds). *Advances in smart coatings and thin films for future industrial and biomedical engineering applications*, Amsterdam, Oxford, Cambridge, Elsevier, p 57–97.
- Soares BMC, Dantas ST, Anjos CAR (2017) Corrosion of aluminum for beverage packaging in acidic media containing chlorides and copper ions. *J Food Process Eng* 40(6):e12571. <https://doi.org/10.1111/jfpe.12571>
- Hou B et al. (2017) The cost of corrosion in China. *npj Mater Degrad* 1(1 Dec):4. <https://doi.org/10.1038/s41529-017-0005-2>
- Al Zubaidy EAH, Mohammad FS, Bassioni G (2011) Effect of pH, salinity and temperature on aluminum cookware leaching during food preparation. *Int J Electrochem Sci* 6(12):6424–6441
- Alabi OA, Adeoluwa YM (2020) Production usage, and potential public health effects of aluminum cookware: a review. *Ann Sci Technol* 5(1):20–30. <https://doi.org/10.2478/ast-2020-0003>
- Inan-Eroglu E, Gulec A, Ayaz A (2019) Effects of different pH, temperature and foils on aluminum leaching from baked fish by ICP-MS. *Czech J Food Sci* 37(3):165–172. <https://doi.org/10.17221/85/2018-CJFS>
- Klotz K, Weistenhöfer W, Neff F, Hartwig A, van Thriel C, Drexler H (2017) The health effects of aluminum exposure. *Dtsch Aertzblatt Online* 114(39 Sep):653–659. <https://doi.org/10.3238/arztebl.2017.0653>
- Exley C (2013) Human exposure to aluminium. *Environ Sci Process Impacts* 15(10):1807–1816. <https://doi.org/10.1039/C3EM00374D>
- Li K, Kou H, Ning C (2021) Sintering and mechanical properties of lithium disilicate glass-ceramics prepared by sol-gel method. *J Non Cryst Solids* 552:120443. <https://doi.org/10.1016/j.jnoncrsol.2020.120443>
- Jelle BP, Baetens R, Gustavsen A (2015) Aerogel insulation for building applications. In: Levy D, Zayat M (eds) *The sol-gel handbook*. Wiley-VCH Verlag GmbH & Co. KGaA, Weinheim, p 1385–1412
- Figueira RB, Silva CJR, Pereira EV (2015) Organic–inorganic hybrid sol–gel coatings for metal corrosion protection: a review of recent progress. *J Coat Technol Res* 12(1 Jan):1–35. <https://doi.org/10.1007/s11998-014-9595-6>
- GahremanDerakhshan M, Nikzad L, Farvizi M, Ebadzadeh T (2020) Sol-gel assisted synthesis of TiB₂-B₄C composite powder. *Int J Appl Ceram Technol* 18(2021):32–39. <https://doi.org/10.1111/jjac.13615>
- Yona AMC, Žigon J, Dahle S, Petric M (2021) Study of the adhesion of silicate-based coating formulations on a wood substrate. *Coatings* 11:1. <https://doi.org/10.3390/coatings11010061>
- Adaka D, Bhattacharyya R, Saha H, Maiti PS (2020) Sol-gel processed silica based highly transparent self-cleaning coatings for solar glass covers. *Mater Proc* 33(6):2429–2433. <https://doi.org/10.1016/j.matpr.2020.01.331>
- Purcar V et al. (2020) Preparation and characterization of some sol-gel modified silica coatings deposited on polyvinyl chloride (PVC) substrates. *Coatings* 11(1 Dec):11. <https://doi.org/10.3390/coatings11010011>
- Hench LL, West JK (1990) The sol-gel process. *Chem Rev* 90(1):33–72. <https://doi.org/10.1021/cr00099a003>

18. Brinker CC, Scherer GW (1990) Sol-gel science: the physics and chemistry of sol-gel processing. Academic Press, INC, Boston, San Diego, New York, NY, London, Sydney, Tokyo, Toronto
19. Rodič P, Milošev I, Lekka M, Andreatta F, Fedrizzi L (2018) Corrosion behaviour and chemical stability of transparent hybrid sol-gel coatings deposited on aluminium in acidic and alkaline solutions. *Prog Org Coat* 124(Nov):286–295. <https://doi.org/10.1016/j.porgcoat.2018.02.025>
20. Rodič P, Iskra J, Milošev I (2014) A hybrid organic-inorganic sol-gel coating for protecting aluminium alloy 7075-T6 against corrosion in Harrison's solution. *J Sol-Gel Sci Technol* 70 (1):90–103. <https://doi.org/10.1007/s10971-014-3278-8>
21. Milošev I, Kapun B, Rodič P, Iskra J (2015) Hybrid sol-gel coating agents based on zirconium(IV) propoxide and epoxysilane. *J Sol-Gel Sci Technol* 74(2 May):447–459. <https://doi.org/10.1007/s10971-015-3620-9>
22. Rodič P, Iskra J, Milošev I (2014) Study of a sol-gel process in the preparation of hybrid coatings for corrosion protection using FTIR and ¹H NMR methods. *J Non Cryst Solids* 396–397 (Aug):25–35. <https://doi.org/10.1016/j.jnoncrysol.2014.04.013>
23. Schubert U (2003) Silica-based and transition metal-based inorganic-organic hybrid materials—a comparison. *J Sol-Gel Sci Technol* 26(1/3):47–55. <https://doi.org/10.1023/a:1020729100148>
24. Schubert U (2007) Organically modified transition metal alkoxides: chemical problems and structural issues on the way to materials syntheses. *Acc Chem Res* 40(9):730–737. <https://doi.org/10.1021/ar600036x>
25. Del Monte F, Cheben P, Grover CP, Mackenzie JD (1999) Preparation and optical characterization of thick-film zirconia and titania ormosils. *J Sol-Gel Sci Technol* 15:73–85. <https://doi.org/10.1023/A:1008717215060>
26. Jeon BY, Kim SM (2007) Non-stick ceramic coating composition and process. US Patent 20070218297 A1
27. Uğur MH, Çakmakçı E, Güngör A, Kayaman-Apohan N (2018) Surface properties of sol-gel-based fluorine-containing ceramic coatings. *J Sol-Gel Sci Technol* 87(1):113–124. <https://doi.org/10.1007/s10971-018-4713-z>
28. Baney RH, Chi FK (1981) Pigment-free coatings with improved resistance to weathering. US Patent 4275118A
29. Figueira RB (2020) Hybrid sol-gel coatings for corrosion mitigation: a critical review. *Polymers* 12(3 Mar):689. <https://doi.org/10.3390/polym12030689>
30. Carre A, Prassas M, Waku-Nsimba J (2000) Coating for imparting non-stick, abrasion resistant and non-wetting properties to inorganic articles. US Patent 6054522A
31. Jirathampradhab T, Lhosupasirirat S, Kumnorkeaw P, Akhadejdamrong T, Rojanapitayakorn P, Sriksirin T (2017) Study the effect of coating thickness from silica nanocomposite deposited on poly(methyl methacrylate) sheets via spray coating technique. *Mater Sci Forum* 895(Mar):79–82. <https://doi.org/10.4028/www.scientific.net/MSF.895.79>
32. Clark HA (1976) Pigment-free coating compositions. US Patent 3986997A
33. Kanokwijitsilp T, Traiperm P, Osotchan T, Sriksirin T (2016) Development of abrasion resistance SiO₂ nanocomposite coating for teak wood. *Prog Org Coat* 93(Apr):118–126. <https://doi.org/10.1016/j.porgcoat.2015.12.004>
34. Huhtamäki T, Tian X, Korhonen JT, Ras RHA (2018) Surface-wetting characterization using contact-angle measurements. *Nat Protoc* 13(7 Jul):1521–1538. <https://doi.org/10.1038/s41596-018-0003-z>
35. Enev V, Sedláček P, Jarábková S, Velcer T, Pekař M (2019) ATR-FTIR spectroscopy and thermogravimetry characterization of water in polyelectrolyte-surfactant hydrogels. *Colloids Surf A Physicochem Eng Asp* 575(Aug):1–9. <https://doi.org/10.1016/j.colsurfa.2019.04.089>
36. Armelao L et al. (2007) Highly dispersed mixed zirconia and hafnia nanoparticles in a silica matrix: first example of a ZrO₂-HfO₂-SiO₂ ternary oxide system. *Adv Funct Mater* 17(10 Jul):1671–1681. <https://doi.org/10.1002/adfm.200600458>
37. Hanom Binti Rashid S, Synthesis, characterisation and corrosion protection performance of hybrid nanocomposite coatings. Manchester, University of Manchester, 2020.
38. Gonzalez E, Vejar N, Solis R, Muñoz L, Victoria Encinas M, Paez M (2019) Sol-gel films: corrosion protection coating for aluminium alloy. In: Valverde Aguilar Guadalupe (ed) Sol-gel method - design and synthesis of new materials with interesting physical, chemical and biological properties. IntechOpen, London
39. Li CQ, Zhu MY, Ou JF, Lu YL, Wang FJ, Li W (2018) Dynamic corrosion behavior of superhydrophobic surfaces. *RSC Adv* 8 (51):29201–29209. <https://doi.org/10.1039/C8RA05200J>
40. Somorjai GA, Li Y (2010) Introduction to surface chemistry and catalysis, second edition. John Wiley&Sons, Inc, New Jersey
41. Bunker BC et al. (2002) Hydration of passive oxide films on aluminum. *J Phys Chem B* 106(18 May):4705–4713. <https://doi.org/10.1021/jp013246e>
42. Wang D, Bierwagen GP (2009) Sol-gel coatings on metals for corrosion protection. *Prog Org Coat* 64(4 Mar):327–338. <https://doi.org/10.1016/j.porgcoat.2008.08.010>
43. Villegas MA (2001) Chemical and microstructural characterization of sol-gel coatings in the ZrO₂-SiO₂ system. *Thin Solid Films* 382(1–2):124–132. [https://doi.org/10.1016/S0040-6090\(00\)01698-9](https://doi.org/10.1016/S0040-6090(00)01698-9)
44. Zhan Z, Zeng HC (1999) A catalyst-free approach for sol-gel synthesis of highly mixed ZrO₂-SiO₂ oxides. *J Non Cryst Solids* 243(1):26–38. [https://doi.org/10.1016/S0022-3093\(98\)00810-2](https://doi.org/10.1016/S0022-3093(98)00810-2)
45. Hauli L, Wijaya K, Armunanto R (2018) Preparation and characterization of sulfated zirconia from a commercial zirconia nanopowder. *Orient J Chem* 34(3 Jun):1559–1564. <https://doi.org/10.13005/ojcc/340348>
46. Reyes-Acosta MA, Torres-Huerta AM, Domínguez-Crespo MA, Flores-Vela AI, Dorantes-Rosales HJ, Ramírez-Meneses E (2015) Influence of ZrO₂ nanoparticles and thermal treatment on the properties of PMMA/ZrO₂ hybrid coatings. *J Alloy Compd* 643 (Sep):150–158. <https://doi.org/10.1016/j.jallcom.2014.10.040>
47. Jankauskaitė V, Narmontas P, Lazauskas A (2019) Control of polydimethylsiloxane surface hydrophobicity by plasma polymerized hexamethyldisilazane deposition. *Coatings* 9(Jan):36. <https://doi.org/10.3390/coatings9010036>
48. Kumar D et al. (2015) Hydrophobic sol-gel coatings based on polydimethylsiloxane for self-cleaning applications. *Mater Des* 86 (Dec):855–862. <https://doi.org/10.1016/j.matdes.2015.07.174>
49. Liu S et al. (2015) Self-cleaning transparent superhydrophobic coatings through simple sol-gel processing of fluoroalkylsilane. *Appl Surf Sci* 351(Oct):897–903. <https://doi.org/10.1016/j.apsusc.2015.06.016>
50. Izumi K et al. (1990) Coating of fluorine-doped ZrO₂ films on steel sheets by sol-gel method. *J Non Cryst Solids* 121(1–3 May):344–347. [https://doi.org/10.1016/0022-3093\(90\)90156-G](https://doi.org/10.1016/0022-3093(90)90156-G)
51. Leloup FB, Audenaert J, Obein G, Ged G, Hanselaer P (2016) Repeatability and reproducibility of specular gloss meters in theory and practice. *J Coat Technol Res* 13(6 Nov):941–951. <https://doi.org/10.1007/s11998-016-9813-5>
52. Torrico RFAO et al. (2018) Structure and properties of epoxy-siloxane-silica nanocomposite coatings for corrosion protection. *J Colloid Interface Sci* 513(Mar):617–628. <https://doi.org/10.1016/j.jcis.2017.11.069>
53. WU LYL, Tan GH, Zeng XT, Li TH, Chen Z (2006) Synthesis and characterization of transparent hydrophobic sol-gel hard coatings. *J Sol-Gel Sci Technol* 38(1):85–89. <https://doi.org/10.1007/s10971-006-5917-1>

54. Zang X et al. (2012) One-step sol–gel preparation of PDMS–silica ORMOSILs as environment-resistant and crack-free thick antireflective coatings *J Mater Chem* 22:13132–13140. <https://doi.org/10.1039/c2jm31005h>
55. Suriano R, Ciapponi R, Grif G, Levi M, Turri S (2017) Fluorinated zirconia-based sol-gel hybrid coatings on polycarbonate with high durability and improved scratch resistance. *Surf Coat Technol* 311:80–89. <https://doi.org/10.1016/j.surfcoat.2016.12.095>
56. Armelao L et al. (2005) Zirconium and hafnium oxoclusters as molecular building blocks for highly dispersed ZrO₂ or HfO₂ nanoparticles in silica thin films. *J Mater Chem* 15 (18):1838–1948. <https://doi.org/10.1039/b500521c>
57. Maleki H, Durães L, García-González CA, del Gaudio P, Portugal A, Mahmoudi M (2016) Synthesis and biomedical applications of aerogels: possibilities and challenges. *Adv Colloid Interface Sci* 236(Oct):1–27. <https://doi.org/10.1016/j.cis.2016.05.011>
58. Mahadik SA et al. (2013) Superhydrophobic silica coating by dip coating method. *Appl Surf Sci* 277(Jul):67–72. <https://doi.org/10.1016/j.apsusc.2013.04.001>